ACS Catalysis

pubs.acs.org/acscatalysis
Research Article

Shortening Accelerated Stress Tests: An Identical Charge Approach for Oxygen Evolution Reaction Electrocatalysts

Philipp L. Darge,* Nico C. Röttcher, Matej Zlatar, Karl J. J. Mayrhofer, Serhiy Cherevko, and Dominik Dworschak*

Cite This: ACS Catal. 2025, 15, 10336−10346
Read Online

ACCESS | Metrics & More | Article Recommendations | Supporting Information

ABSTRACT: Proton exchange membrane water electrolysis (PEMWE) is expected to play a major role in hydrogen production due to its suitability for dynamic response and load flexibility, which are relevant for operation with electricity from fluctuating renewables. A central problem is however the loading reduction of scarce and expensive iridium, which is needed to catalyze the sluggish oxygen evolution reaction (OER) on the anode while maintaining activity and stability. To accelerate improvements on the anode catalyst side, it is central to evaluate electrocatalyst stability fast and to assess its suitability for dynamic operation. In this study, we evaluate the possibility of reducing the time for stability screening of a commercial iridium oxide catalyst by using a constant charge approach, which is desirable to enable high throughput screening. The approach is inspired by the relationship between OER and the dissolution mechanism. For this, a scanning flow cell with online inductively coupled plasma mass spectrometry (SFC-ICP-MS) is used to measure time-resolved iridium dissolution. Further, the impact of dynamic stress protocols on degradation is assessed. For this, a static current hold is fragmented into square wave protocols using shorter start−stop cycles while maintaining the cumulative time under current and total applied charge. Our results show that an acceleration of testing can be achieved while the total dissolution per charge remains similar. The choice of pulsing parameters critically affected catalyst dissolution and inconsistencies with full cell degradation trends in literature revealed the need to consider pseudocapacitive current contributions.

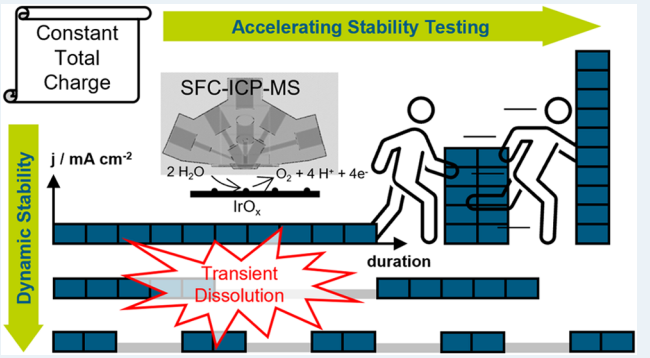

KEYWORDS: *oxygen evolution reaction, iridium oxide, accelerated stress test, dissolution, stability benchmarking*

1. INTRODUCTION

High expectations weigh on green hydrogen production via electrolysis for the decarbonization of various industries and load management of intermittent renewable energy sources.[1] Currently, however, only about 4% of the globally produced hydrogen is obtained electrically via water electrolysis, while the majority is produced by fossil fuel-based methods like steam methane reforming.[2,3] Among different technologies, proton exchange membrane water electrolysis (PEMWE) is considered a promising technology for large-scale implementation in combination with renewable energy sources.[1] This is because PEMWE allows for high relative current densities, fast load changes, and has a higher maturity than anion exchange membrane water electrolysis (AEMWE).[1,4] But high costs and limited stability still impede scale-up.[5] Catalyst-wise, especially the reduction of scarce and expensive iridium on the anode side for the sluggish oxygen evolution reaction (OER) without affecting activity and lifetime remains challenging due to the harsh oxidative conditions.[1] The targets of the US Department of Energy (DOE) for 2026 are to reduce the total catalyst loading to 0.5 mg_{PGM} cm^{-2} (2022:3 mg_{PGM} cm^{-2}) and double the operation lifetime to 80k h in PEMWE.[6] But to reach these targets, further improvements in electrocatalyst performance are needed.

Due to the high required effort/time and the complexity of full cell testing, OER electrocatalysts are initially tested on the material level in aqueous model systems (AMS), typically using a rotating disc electrode (RDE) or scanning flow cell with online inductively coupled plasma mass spectrometry (SFC-ICP-MS). Additionally, AMS can be used for high throughput screening via process automation, which allows the discovery of larger material and parameter spaces.[7−10] Complementary to automation, the reduction of time required for the electrochemical testing is needed to increase throughput.

Received: February 25, 2025
Revised: May 26, 2025
Accepted: May 27, 2025
Published: June 2, 2025

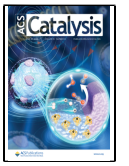

https://doi.org/10.1021/acscatal.5c01464
ACS Catal. 2025, 15, 10336−10346

However, because AMS simplify and change the testing environment and components found in a full cell, the observed behavior can deviate from that under realistic conditions.[5] Disagreements were e.g., found for activity trends of different iridium oxide catalysts in SFC versus membrane electrode assemblies (MEAs) due to differences in catalyst utilization and mass transport properties for the thinner catalyst layers in AMS.[11] These activity trends were however found to uphold after high-frequency resistance (HFR) correction, showing that AMS can give valuable information about the activity as a pure material property.

Stability on the full cell level is typically measured by characterizing the loss of electrochemical performance over time due to the degradation of all components and interfaces. Since the measurement setup and operating conditions differ significantly between AMS and MEA, it has been discussed how valuable electrochemical measurements in AMS are for stability characterization.[5,12] Further, concerning the measurement of electrochemical performance losses in AMS, component behavior in model setups was found to affect measurement results. The passivation of the support material, especially glassy carbon, has been shown to lead to significantly elevated overpotentials during OER over time compared to other substrate materials like gold.[13,14] Further, the accumulation of oxygen microbubbles, leading to increasing blockage of active sites has been discussed to cause increased activity losses in AMS compared to MEA.[15−19] Hence, the use of electrochemical performance loss to characterize OER electrocatalyst degradation in AMS has to be evaluated carefully.

Simultaneously, iridium dissolution has been increasingly discussed as an important factor for performance losses in MEAs and was investigated on both full-cell and AMS levels.[1,4,5,11,12,20−33] This is because catalyst dissolution as a primary degradation mechanism leads to thinning of the anode catalyst layer, adding to kinetic losses, and is estimated to dominate MEA performance degradation over long-term operation.[12,26] The investigation of losses in full cells has progressed toward understanding the complex behavior of dissolved catalyst ions and their effects on other components and interfaces and their performance. Here, the migration of dissolved iridium ions into the membrane and slower kinetics due to bad catalyst/ionomer integration and catalyst/membrane interface weakening are deemed important.[31,33] It was further shown in a full cell that after an accelerated stress test (AST), the majority of dissolved iridium was not found in the water lines but migrated into the membrane and redeposited on the cathode catalyst layer.[29] This is a significant mechanistic difference compared to the straightforward study of dissolution in AMS, where the catalyst layer is typically immersed in a liquid electrolyte, into which the catalyst material can simply dissolve without causing secondary effects.

On a fundamental level, much progress has been made in understanding the dissolution of iridium-based catalysts as well, finding that high overpotentials (OER) are required to cause iridium dissolution at significant levels due to faster reaction rates.[23] It was shown for iridium and other metals, that transient dissolution due to surface oxidation and reduction processes is one mechanism responsible for catalyst losses.[22,23,34] Additionally, dissolution is triggered by the OER itself and depends on the detailed mechanisms on each surface.[22] OER dissolution is affected by the oxidation state, with more oxidized and anhydrous/crystalline surfaces typically being more stable.[21] The situation is further complicated by the suggestion, that the decrease in dissolution after an initial peak following a current/potential onset is caused by at least partially irreversible electrochemical surface oxidation/passivation processes.[21] Hence it has to be considered, that in addition to the initial oxidation state at the beginning of an experiment, the electrochemical measurement itself will likely change the catalyst surface dynamically over time, affecting further transient and OER related dissolution.

Mechanism-wise, OER dissolution for both metallic and oxidic iridium catalysts has been discussed as a competitive pathway of the OER reaction mechanism, sharing reaction intermediates.[23,25,34,35] This is further supported by experimental findings from Geiger et al., showing that the S-number (amount of oxygen evolved per iridium dissolved at steady state dissolution during current holds) remained in the same order of magnitude over a broad range of current densities, particularly for iridium oxide.[25] Based on their observation of a positive correlation between iridium dissolution and OER current, they suggested a direct relationship between OER reaction and iridium dissolution mechanism.

Over the past years, accelerated stress/degradation tests (ASTs/ADTs) have received significant attention to characterize OER electrocatalyst degradation under dynamic conditions.[4,12,20,21,24,27,35] Different protocol approaches can be found, like the application of CVs or square wave CA/CP protocols to simulate dynamic operation and investigate the effects of parameter variations on catalyst stability.

Alia et al. implemented a stress test based on CVs, comparing RDE batch dissolution of iridium and iridium oxide particles from static potential holds to dissolution after CVs, choosing 1.4 V vs RHE as lower potential limit (LPL) and different upper potential limits (UPLs).[12] The protocols used had an identical duration of 13.5 h for holds and CVs (30k cycles, scan rate adjusted with UPLs for 13.5 h duration). It was found that holds caused higher dissolution than the CV-based ASTs for both metallic and oxidic samples with differences increasing with the applied UPLs up to 2 V vs RHE. This shows that dynamic protocols when based on CVs, where only a fraction of the protocol duration is spent at elevated potentials, do not necessarily accelerate catalyst dissolution compared to a simple hold over the same duration. Further, a positive correlation between dissolution and activity losses in RDE was found for iridium nanoparticles, not however for oxidic samples.[12,31]

A different approach based on 3/3 s square wave potential cycles was proposed by Spöri et al., similar to a previous 3/3 s square wave current AST used by Cherevko et al. with a SFC.[21,27,35] Spöri et al. used alternating CA steps at 0.05 V vs RHE and different UPLs (1.4−2.0 V vs RHE) with durations of 3/3 s for 15k cycles (25 h) in RDE.[27,35] They found that for iridium oxide, obtained from spin coating iridium acetate on Ti-discs and a calcination step at 300 °C, dissolution after their ASTs was increased compared to static CA holds during which only the UPL was applied for 25 h without interrupts. The increased dissolution after their AST was observed for all UPLs from 1.4 to 2.0 V vs RHE even though during the AST only half of the 25 h were spent at OER relevant potentials. An important difference in the protocols used by Spöri et al. compared to the CVs applied by Alia et al. is the used LPL. It was shown for metallic iridium and its hydrous oxide and for both potential sweeps and holds, that LPLs down into the range of 0 V vs RHE significantly affect the contribution of

https://doi.org/10.1021/acscatal.5c01464
ACS Catal. 2025, 15, 10336−10346

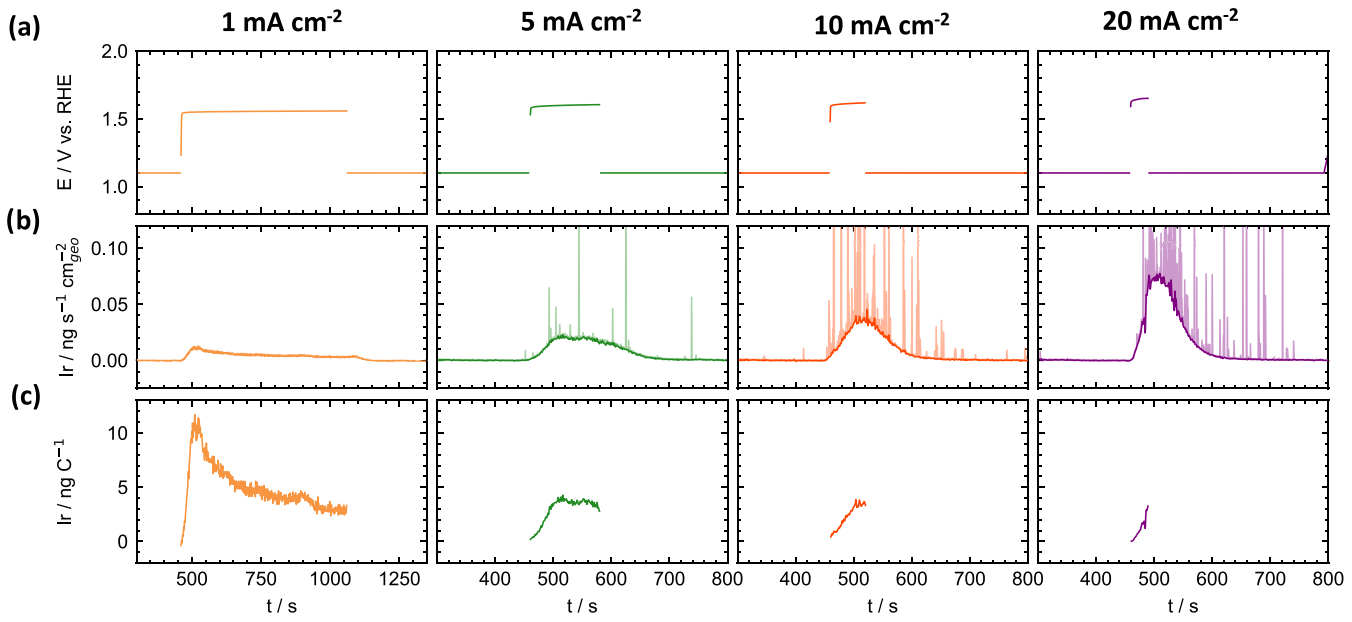

Figure 1. Electrochemical online dissolution profiles of iridium oxide using SFC-ICP-MS for static stress tests during which the total applied charge was controlled. (a) Measured potentials as the result of current holds at 1 mA cm^{-2} × 600 s, 5 mA cm^{-2} × 120 s, 10 mA cm^{-2} × 60 s, and 20 mA cm^{-2} × 30 s. (b) Contributions from underlying electrochemical dissolution and dissolution spikes (detachment) were deconvoluted. (c) Iridium dissolution normalized to the applied current densities during each CP hold giving the iridium per charge ratio.

cathodic transient dissolution due to the reduction of the oxidized catalyst surface.[23,34] Based on this, cathodic dissolution would not yet be expected for LPLs around 1.4 V vs RHE, as used by Alia et al., which is one possible reason why their CVs did not increase dissolution compared to a simple hold.

The effect of LPLs and support materials on iridium black dissolution was further investigated by Zlatar et al. applying a 3/3 s square wave potential cycling protocol, similar to Spöri et al., with UPLs of 1.6 V vs RHE in a SFC-ICP-MS.[4] They found that dissolution increased as the LPL decreased from 1.4 V vs RHE to 0.9−1.23 V vs RHE simulating a standby step. The highest dissolution was found at LPLs of 0 V vs RHE, which was used to simulate hydrogen crossover conditions. Additionally, iridium dissolution significantly increased on gold compared to glassy carbon or iridium oxide (with dissolution correction), showing that gold substrates can affect dissolution studies for dynamic protocols.[4] This observation of increased iridium dissolution on gold during dynamic protocols also matches with findings in RDE by Alia et al.[12]

While progress has been made in understanding iridium dissolution due to different dynamic potential conditions, studies typically compare whether ASTs increase dissolution within the same time, leaving possibilities to reduce the time needed for testing unexplored. Further, step durations and cycling frequencies and their effects on dissolution are not investigated in existing AST proposals, requiring further research.

In this study, we hence investigated the dissolution stability of a commercial iridium oxide OER electrocatalyst using an electrochemical SFC-ICP-MS. By applying accelerated static measurement protocols, our results show the potential to further shorten stability screenings while maintaining the total dissolution. Further, we demonstrate that the choice of step durations and cycling frequency as a fundamental parameter for ASTs in AMS critically affects the dissolution of iridium oxide and can even decrease catalyst dissolution. This shows that step durations need to be considered when designing dynamic stress tests for the characterization of OER electrocatalyst stability.

2. EXPERIMENTAL SECTION

2.1. Electrode Preparation. For electrochemical online SFC-ICP-MS measurements, catalyst coatings were prepared from iridium oxide powder (Alfa Aesar). Catalyst inks with a concentration of 0.825 μg_{Ir} mg^{-1} were prepared by creating a mixture of 87.5 vol % ultrapure water (Merck, Milli-Q, 18 MΩ, TOC < 5 ppb) and 12.5 vol % isopropanol (Sigma-Aldrich, ≥99.5%) and adding 5 μL of Nafion perfluorinated resin solution (Sigma-Aldrich, 5 wt %, 1100 W) per mg of catalyst powder as binder. The ink was homogenized in an ice bath using an ultrasonic horn (Branson, SFX150) for 15 min (4 s on/2 s off pulses) at 40% intensity. Subsequently, the pH was adjusted to ∼11 by adding 1 M KOH. Catalyst spots were produced on a polished glassy carbon plate (HTW, Sigradur G) and an Au foil plate (Thermo Fisher Scientific, 99.95%). For this, the freshly prepared ink was drop cast using volumes of 0.2 μL with a half automated process utilizing linear stages and approaching tip-to-surface distances of ∼0.7 mm for stripping of droplets. This led to estimated catalyst loadings of ∼15 μg_{Ir} cm^{-2}. The time between sample preparation and measurements was always kept below 7 days to achieve a good reproducibility of dissolution data.

2.2. Electrochemical Online SFC-ICP-MS Measurements. Electrochemical measurements were performed using a scanning flow cell with online inductively coupled plasma mass spectrometry (SFC-ICP-MS) for elemental analysis. The scanning flow cell used was designed based on the versions already published elsewhere and CNC manufactured from polycarbonate.[36−39] Main channel diameters of 2 mm were used, intersecting at an angle of 60°. The tube connections to the SFC were realized using threaded fittings of the miniature inert tubing system MINSTAC (The Lee Company). Further,

https://doi.org/10.1021/acscatal.5c01464
ACS Catal. 2025, 15, 10336−10346

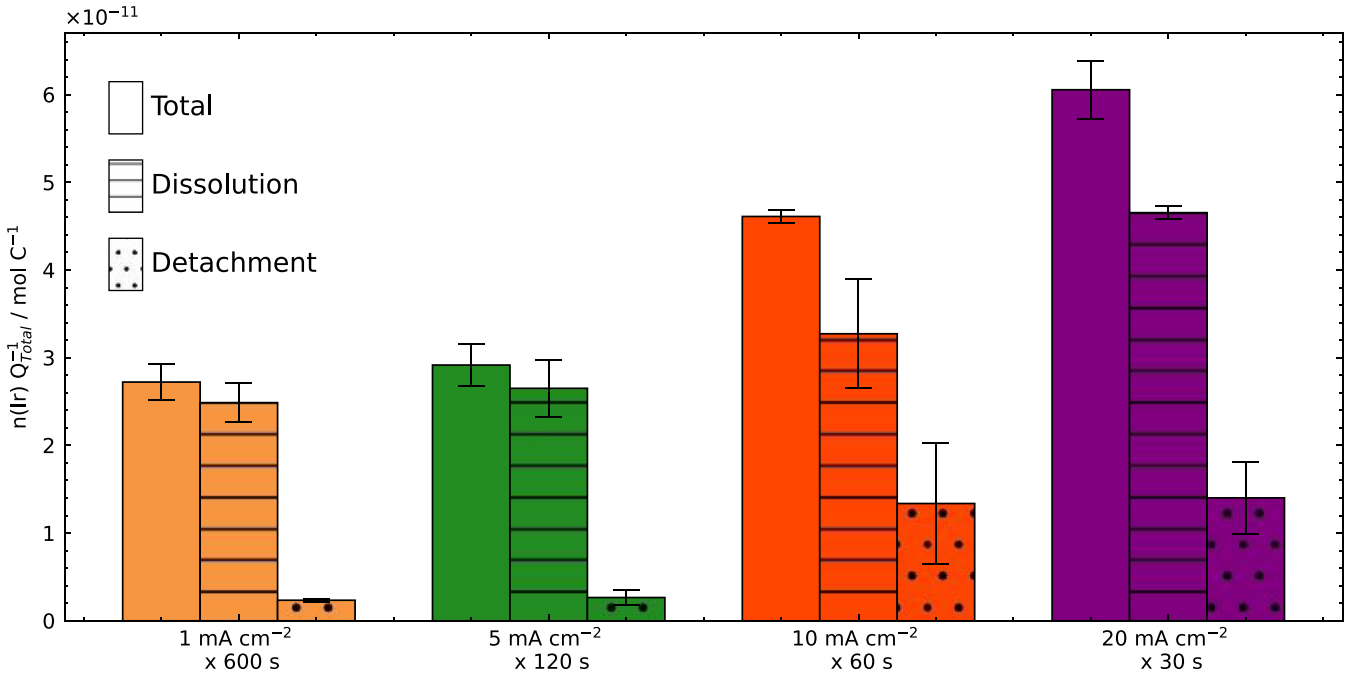

Figure 2. Total iridium dissolution per charge from different static stress tests. The dissolution was integrated over the whole peak area related to the CP holds in Figure 1b. The total dissolution was deconvoluted into contributions from the underlying electrochemical dissolution and spikes detected in the ICP-MS signal. Standard deviations were calculated from the deviations between measurements.

PTFE/PEEK compartments were developed that enabled the direct use of a screwable mini-Hydroflex RHE (Gaskatel), connected to the SFC inlet as a reference electrode (RE). A similar compartment was manufactured for a screwable glassy carbon counter electrode (CE), based on a 1.6 mm glassy carbon rod (HTW, Sigradur G) and PEEK flangeless fittings with UNF-1/4−28 threads.

Electrochemical online dissolution measurements were conducted using Ar-purged 0.1 M $HClO_4$, which was prepared freshly for every measurement by diluting concentrated $HClO_4$ (Suprapure 70%, Roth) and ultrapure water (18 MΩ, TOC < 5 ppb). The electrolyte flow from an electrolyte reservoir through the SFC main channels into the ICP-MS (Agilent 7900) was established by connecting the SFC outlet to the peristaltic pump of the ICP-MS.

Before entering the ICP-MS, the electrolyte from the sample tube was mixed with the internal standard using a T-piece. The electrolyte (sample) flow rate was experimentally measured to be approximately 340 μL min^{-1} across all experiments. As an internal standard, a 3 $\mu g\ l^{-1}$ Re solution was used, which was produced daily by diluting a 10 mg l^{-1} stock solution with freshly prepared electrolyte. The ICP-MS was tuned and calibrated daily using solutions with Ir and Au concentrations of 0.5, 1, and 5 $\mu g\ l^{-1}$ Ir diluted from 10 mg l^{-1} stock solutions with freshly prepared electrolyte. Stock solutions (10 mg l^{-1}) for internal standards (Re) and calibration (Ir, Au) were produced from commercial ICP standard solutions (Certipur 1000 mg l^{-1}, Merck) and 2 wt % HNO_3 prepared from concentrated HNO_3 (Suprapure 69%, Roth) and ultrapure water (18 MΩ, TOC < 5 ppb).

For electrochemical online dissolution measurements, the working electrode (catalyst spot drop cast on glassy carbon or gold) was placed on an *XYZ* linear stage. Electrochemical measurements were conducted using a Gamry (Reference 620) potentiostat.

3. RESULTS AND DISCUSSION

3.1. Effects of Reduced Measurement Durations and Elevated Current Densities on Degradation. To investigate the effects of reduced protocol durations on dissolution and the possibility of reducing the time required for OER stability screening, a variation of static stress tests using chronopotentiometric (CP) steps at different current densities was applied, as visible in Figure 1. Stress tests were designed to keep the exchanged charge constant so that when the duration decreased, the current density increased in exchange (e.g., 1 mA cm^{-2} × 600 s, 5 mA cm^{-2} × 120 s). LSVs were used to characterize activity before and after each static stress test. The full protocol descriptions and electrochemical results are available in the Supporting Information (SI) and Figures S1−S3. This controlled total charge approach was chosen since a direct relationship between OER current and iridium dissolution was already suggested before.[25]

Generally, the maximum dissolution rates in Figure 1b increased with the applied current density, which is consistent with the suggestion of a direct relationship between dissolution and the OER reaction mechanism. For the 1 mA cm^{-2} hold for 600 s, the characteristic dissolution profile can still be observed. Together with the current onset, the dissolution increased as well, peaking at a maximum. As previously discussed, this initial dissolution is likely the result of both transient and OER-related dissolution. Transient dissolution due to further surface oxidation seems reasonable also when considering that peaks similar to the metallic fcc structure of iridium are still predominant in the XRD pattern of the used iridium oxide (Alfa Aesar).[40] Both the crystallographic properties and dissolution rate of the used material at 1 mA cm^{-2} match well with results from iridium oxides obtained from thermal oxidation at 300−400 °C where no stoichiometric oxide is obtained.[21,40]

https://doi.org/10.1021/acscatal.5c01464
ACS Catal. 2025, 15, 10336−10346

After that, the dissolution rate exponentially decays as the material stabilizes until a quasi-steady state is approximated. The decrease in dissolution rate over time has already before been attributed to irreversible surface passivation processes for different iridium oxides.[21]

For the other current holds, the durations (30−120 s) are too short to observe significant stabilization or approximation of steady state dissolution. It is, however, visible, that a similar exponential decrease in dissolution and approximation of steady state levels would also occur at higher current densities, as e.g., shown for 3 and 5 mA cm^{-2} in Figure S4.

Further, it can be observed that with increasing current density not only the underlying electrochemical dissolution increased but also the visual density of spikes in the ICP-MS signal. This increase in spikes with increasing current densities occurred simultaneously with an increase of the observed evolution of bubbles from the working electrode, especially at 10 and 20 mA cm^{-2}. We attribute this to the mechanical detachment of particles from the catalyst film. To differentiate between dissolution from underlying electrochemical dissolution and spikes, the dissolution signal was fitted, as visible in Figure 1b.

Additionally, the iridium dissolution rate normalized to the applied current density (dissolution per charge) during each current hold is depicted in Figure 1c. While the absolute dissolution levels increased for larger current densities, the dissolution relative to the applied current did not show the same behavior. Instead, it is visible that the initial dissolution per charge for current densities above 1 mA cm^{-2} was closer to the lower steady state dissolution value reached at the end of the 600 s hold at 1 mA cm^{-2}. A possible reason for the higher initial dissolution rate per current at 1 mA cm^{-2} compared to e.g., 5 mA cm^{-2} could be that at the lower current density, a higher share of the current is initially consumed by surface passivation, leading to relatively more transient dissolution. Because a severalfold increase of the current only slightly affected the measured potential, it is likely that the majority of the additional electrons would participate in the OER rather than further surface oxidation. Figure S4 shows as well, that the S-numbers for holds at 1 and 5 mA cm^{-2} approximate similar values when reaching quasi-steady state, while the initial dissolution per OER current was higher for 1 mA cm^{-2}. The linear correlation between OER current and dissolution hence increased when steady state dissolution was approximated.

The total iridium dissolution per charge can be considered to further analyze the degradation of iridium oxide from the static ASTs, as depicted in Figure 2. The total values were calculated by integrating the dissolution profiles caused by the respective current holds in Figure 1b. Even though the total charge was already defined as identical for all protocols, the additional normalization of dissolution by current should emphasize the relevance of considering the relationship between iridium dissolution and OER.

For the total dissolution, the contributions from the underlying profile were fitted to differentiate between electrochemical dissolution and particle detachment. It is visible that the total dissolution for both the 1 mA cm^{-2} × 600 s and 5 mA cm^{-2} × 120 s measurements was dominated by the electrochemical dissolution. The total dissolution caused by the 5 mA cm^{-2} current hold is only at the level of the 1 mA cm^{-2} hold even though the shorter hold duration limited the passivation of the surface. The reason for the similar calculated total dissolution values is the previously discussed higher initial dissolution rate for 1 mA cm^{-2} visible in Figure 1c. Hence, the reason for the similar dissolution per charge values for 1 and 5 mA cm^{-2} was not the linear relationship between dissolution and OER current as discussed by Geiger et al. for only steady state dissolution but differences in dissolution behavior over time.[25] Due to this, it was possible to maintain dissolution levels while decreasing the duration of the current step. This further highlights the relevance of time-resolved dissolution measurements to gain insight into material degradation behavior.

The total dissolution per charge for the even shorter 10 and 20 mA cm^{-2} current holds increased compared to measurements at 1 or 5 mA cm^{-2}, even though the applied charge (∼0.6 C cm^{-2}) was held constant. The deconvolution of the dissolution signal into underlying electrochemical dissolution and catalyst detachment shows that for 10 and 20 mA cm^{-2} a significant part of this increase can be attributed to the mechanical detachment of particles from the catalyst film. This also matches well with an increase in macroscopic bubble evolution which was observed mainly for 10 and 20 mA cm^{-2}.

The deconvoluted electrochemical dissolution from the 10 mA cm^{-2} stress test is still in a similar range as the values from the 1, and 5 mA cm^{-2} protocols, particularly when considering the error margins. Latest at 20 mA cm^{-2} × 30 s, however, even though the calculated iridium detachment did not change compared to 10 mA cm^{-2}, the total dissolution values are significantly higher compared to all other measurements, even though the total applied charge was not changed. The expected reason for the increase in total electrochemical dissolution per charge with higher current densities and shorter protocol durations would be higher current normalized dissolution rates due to changes in transient dissolution or lack of time for stabilization. Shorter protocols would allow for less passivation of the catalyst surface toward OER dissolution while higher overpotentials might accelerate oxidation. Higher dissolution per charge values for 30 or 60 s versus 120 s are, however, not visible from the time-resolved data in Figure 1c. Instead, the higher total electrochemical dissolution per charge, particularly for 20 mA cm^{-2} × 30 s, is caused by an increasing amount of dissolution that was measured only after the end of the current hold. Hence, further shortening of the current holds while maintaining the total dissolution per charge was limited.

The presented results in Figures 1 and S4 show that for the used catalyst, the application of increasing current densities could be used to manipulate the initial dissolution rates relative to the steady state values. This shows the potential to accelerate catalyst stability testing by reducing the time required to reach steady state dissolution for stability number or dissolution per charge calculation.

The electrochemical activity decay shown in Figure S3 did not correlate well with the degradation measured by dissolution in Figure 2 and was calculated with large relative standard deviations. Especially the small activity losses at 1 mA cm^{-2} compared to 5 mA cm^{-2} and the decreasing electrochemical degradation at 20 mA cm^{-2} do not match with the dissolution results. This suggests that other factors that were not primarily related to dissolution such as surface passivation, oxygen bubble accumulation, or catalyst detachment affected the electrochemically perceived degradation of the used catalyst for these experimental conditions.

While detachment was observed on glassy carbon for a majority of the duration of the current holds at 10 and 20 mA cm^{-2} in Figure 1b and also after the CP steps already ended,

https://doi.org/10.1021/acscatal.5c01464
ACS Catal. 2025, 15, 10336−10346

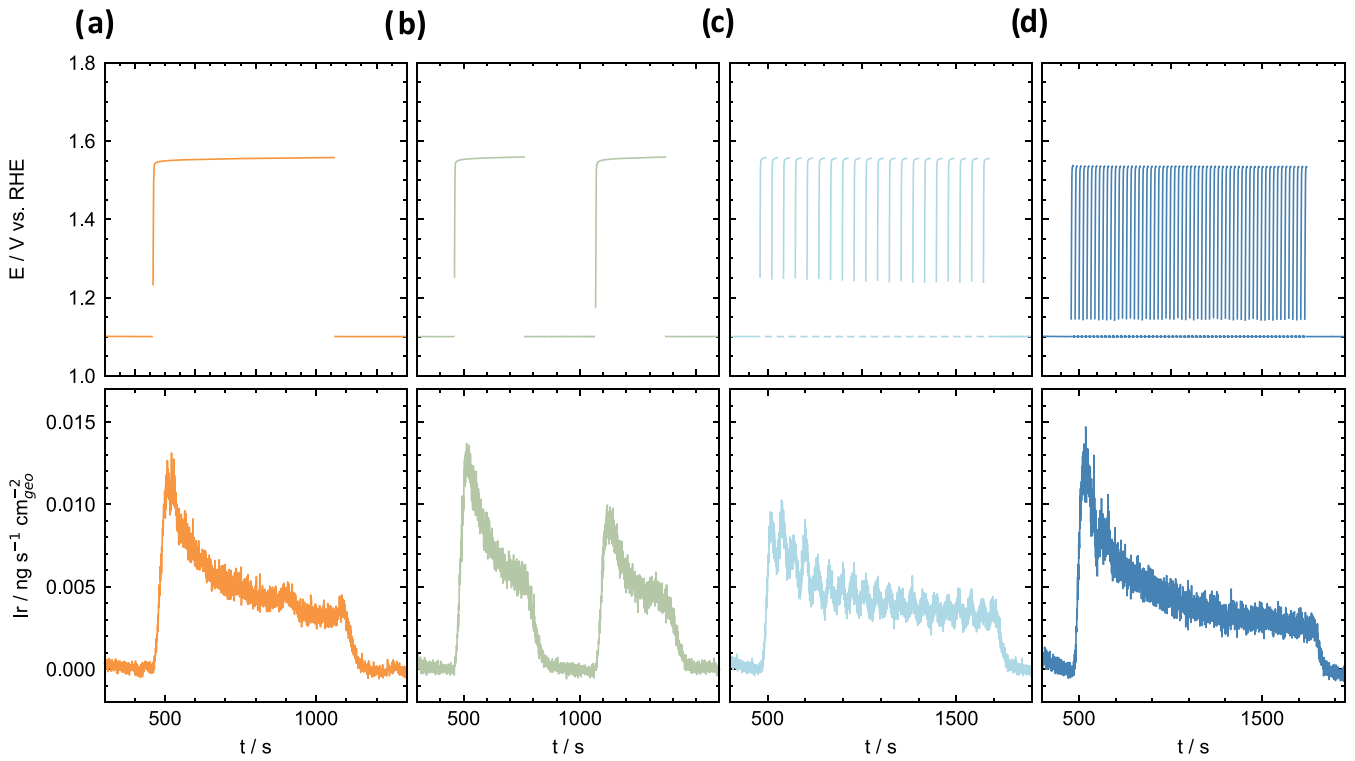

Figure 3. Electrochemical online dissolution measurements of iridium oxide obtained from SFC-ICP-MS for static and dynamic current−potential step protocols. (a−d) Current holds at 1 mA cm^{-2} were interrupted by 1.1 V vs RHE potential holds with identical durations. To control the time under OER current in each stress test, the static stress test was fragmented into shorter CP steps. (a) 600 s × 1, (b) 300 s × 2, (c) 30 s × 20, (d) 10 s × 60. A data set with results from all applied protocols is available in the SI.

this was not observed for the same measurements on a gold substrate. In Figure S5, iridium spikes on gold were only observed together with the maximum electrochemical iridium and gold dissolution. It appears that the detachment depended on the substrate material, potentially due to catalyst film quality, substrate corrosion/passivation, and related interactions between the substrate and catalyst layer.[14,41]

3.2. Impact of Pulse Number and Duration on Degradation. The acceleration of OER electrocatalyst stability screening is desirable and the use of static holds can help to improve standardization of measurements across studies.[14,42] It is however important that also material stability under dynamic conditions is evaluated to investigate the performance of electrocatalysts under fluctuating loads.

To study the impact of operation dynamicity on electrocatalyst degradation during OER, dissolution from static and dynamic protocols with increasing cycling frequency was measured and compared. Figure 3a shows the dissolution from the static stress test, applying 1 mA cm^{-2} × 600 s with the characteristic onset, stabilization, and steady state dissolution phases, already shown in Figure 1. As in the previous measurements on static stress test acceleration, the 1 mA cm^{-2} × 600 s test was used as a benchmark for comparison.

Dynamic stress protocols were defined using the 1 mA cm^{-2} hold for 600 s and fragmenting it into an increasing number of shorter CP steps. These shorter current steps were separated by standby potential holds at 1.1 V vs RHE, leading to different square wave current (Start)−potential (Stop) protocols. The detailed electrochemical protocols can be found in the SI. The number of current steps was adjusted so that the cumulative duration of current holds was kept constant for each stress protocol (600 s × 1, 300 s × 2, 30 s × 20, 10 s × 60, 6 s × 100, 3 s × 200). The potential holds had the same duration as the respective current holds in each measurement, leading to a symmetric square wave protocol with a 50% duty cycle. The potential of 1.1 V vs RHE was chosen as standby potential. Measurement results from the 300 s × 2, 30 s × 20, and 10 s × 60 stress tests are shown in Figure 3b−d, and a complete set of measurement results can be found in Figures S6−S8.

Due to the fragmentation of the single current step into a larger number of shorter steps, dissolution results can be used to evaluate how dissolution stability is affected if oxygen is produced in a single static step or during dynamic loads. This is relevant because in the literature typically dissolution results from protocols are compared that have identical durations but large differences in time under OER-relevant potentials/currents, usually due to different idle periods.[12,20,27] However, since the dissolution of the catalyst—particularly for longer measurements where steady state is approximated—is driven by the OER, considering the total dissolution may lead to over/underestimation of stability. Hence it should be differentiated between ASTs in AMS that aim to accelerate dissolution/degradation within the same period via e.g., dynamic conditions and protocols that are designed for stability comparison under dynamic versus static operation. Lifetime targets in full cells and applied electrolyzers are similarly set for operation time and not standby periods, which needs to be reflected in the conditions the catalyst is exposed to in material tests.[6]

Figure 3b shows the dissolution profile from a stress test with two 1 mA cm^{-2} current steps for 300 s each, interrupted by a 300 s potential step at 1.1 V vs RHE. The two dissolution profiles caused by the OER current holds are still separated, as the time resolution of the used SFC-ICP-MS is sufficient at

https://doi.org/10.1021/acscatal.5c01464
ACS Catal. 2025, 15, 10336−10346

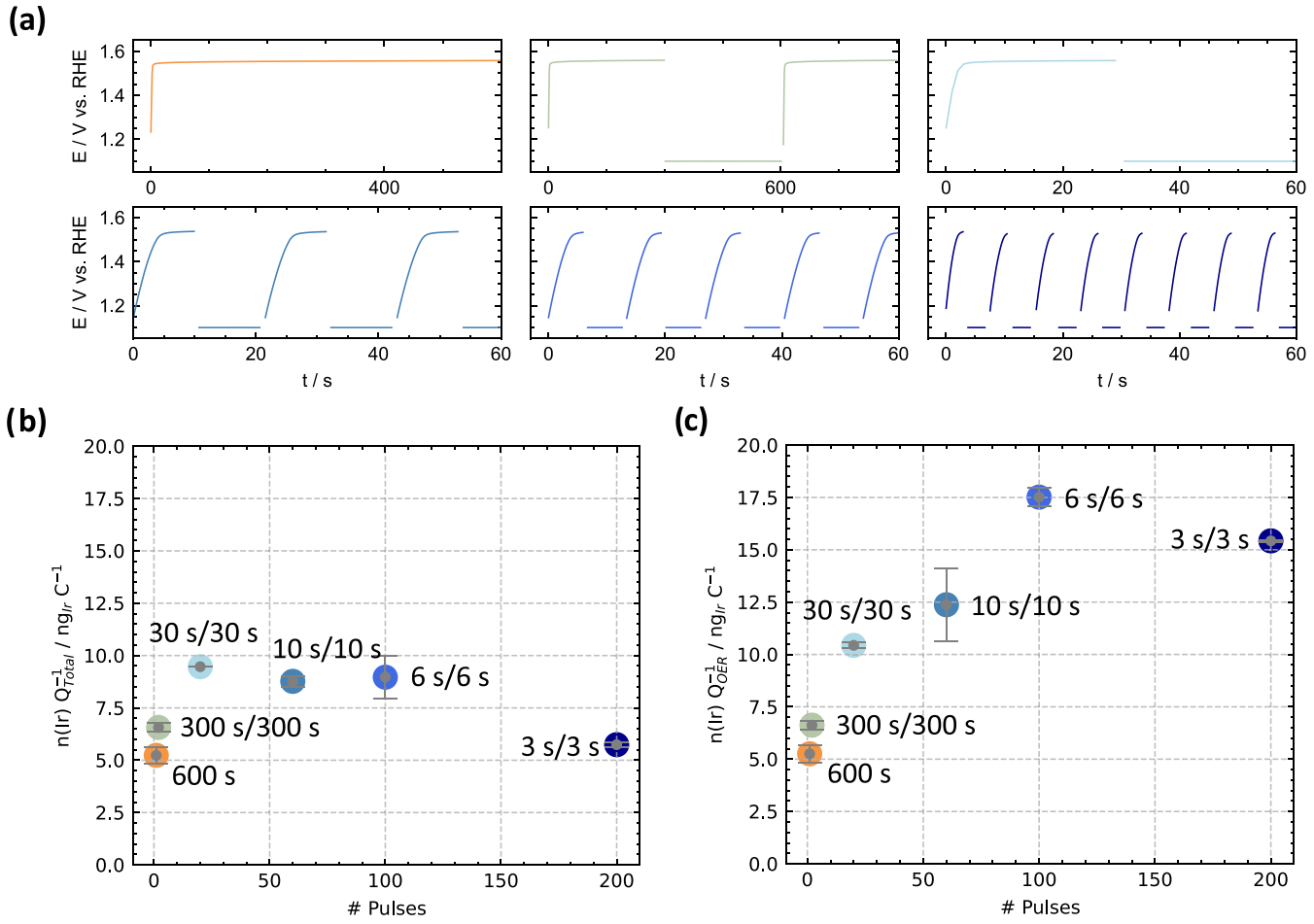

Figure 4. Potential profiles during dynamic stress tests and total iridium dissolution (a) Potential profiles during different stress tests. (b) Total iridium dissolution per total charge in dependence of the number of pulses applied during stress tests with identical durations of applied current. (c) Total iridium dissolution per OER charge after correction for pseudocapacitive contributions.

300 s long steps. The shape of both dissolution signals is similar and follows the typical dissolution onset and subsequent stabilization. Due to the short duration of 300 s per CP step, the dissolution still stabilizes at the end of each current hold, indicating that a longer measurement would be required to approximate steady state. The peak dissolution of the second profile is higher than the dissolution rate at the end of the first CP hold, which shows that the dissolution does not continue from the stabilized level after the current interruption. Instead, the onset of the second current hold caused a spike in dissolution above the previously stabilized level after holding 1 mA cm^{-2} for 300 s for the first time. This could be due to a reductive effect of the 1.1 V vs RHE step and transient dissolution due to the subsequent current step. There is however a lasting stabilization effect visible since the maximum in the second dissolution profile is smaller than the dissolution maximum from the first current hold. The increase in dissolution due to the OER interruption and second current onset with its second peak in dissolution is also quantitatively measurable. The total dissolution from the dynamic 300 s × 2 protocol was 31% higher than during the static 600 s × 1 stress test, reflecting the increase in degradation due to transient conditions. Further, also the memory effect from the stabilization in the first 300 s long current hold in Figure 3b can be quantified, since the second profile only contributed 44% to the dissolution in the 300 s × 2 stress test.

For the stress protocol with 30 s current and potential holds, visible in Figure 3c, the 20 individual dissolution maxima from current holds are still distinguishable. There is however no real peak separation, as the 30 s 1.1 V vs RHE holds are too short. Similar to the dissolution in Figure 3b, each subsequent current onset led to an increase in dissolution rate through the onset of OER current. The maximum of each dissolution peak again decreased over time of the measurement, indicating a stabilization process due to the material's history after each cycle. Overall, an exponential decay of dissolution maxima can be observed, similar to the behavior under static conditions visible in Figure 3a. Toward the end of the measurement, a relatively stable level of dissolution peak maxima was reached, close to steady state dissolution observed for static holds. For the protocol in Figure 3d, during which current and potential holds of 10 s were applied, the individual peaks from current onsets were not distinguishable anymore. But similarly, as in Figure 3c, the dissolution rates still decreased over time with frequent current interrupts and starts, leading to a dissolution profile similar to the curve in Figure 1a.

A detailed depiction of the potential profiles measured during all protocols and the total iridium dissolution values per measured charge can be found in Figure 4. Figure 4b shows that the lowest dissolution per total charge was reached using the static stress protocol at 1 mA cm^{-2} for 600 s. Dynamic stress conditions thus increased catalyst dissolution in all cases.

https://doi.org/10.1021/acscatal.5c01464
ACS Catal. 2025, 15, 10336−10346

The dissolution observed for the 300 s × 2 and 30 s × 20 protocols, where individual peaks are still visible in the dissolution profile, significantly increased compared to the static stress test. With further decreasing current pulse durations to 10 s × 60 and 6 s × 100, the n(Ir) per Q_{total} values stagnated, however, and even decreased slightly. Finally, reducing the current pulse durations to 3 s × 200 significantly decreased the measured dissolution into the range of the static 600 s × 1 protocol. The order of magnitude of the reported changes in total dissolution is comparable to other variations for dynamic protocols recorded using online SFC-ICP-MS.[4] As previously discussed for Figure 3b, the increase in dissolution when transitioning from static to dynamic conditions should be due to transient dissolution caused by each current interruption and onset. The stagnating and decreasing dissolution values per total charge for 10, 6, and 3 s pulses however break this trend. This shows that protocol dynamicity and the number of start−stop cycles are not the only relevant parameters affecting dissolution.

A possible explanation can be found in the electrochemical potential profiles of each stress test, shown in Figure 4a, which are depicted in more detail in Figure S9. It is visible, that approximately 3−6 s are required after each current onset to reach an equilibrated potential. Thus, the relative time under stable potentials for a measurement declined with an increasing number of current pulses of shorter durations. Apart from oxygen bubbles which can block active sites and lead to elevated overpotentials, we suggest that a reason for this is the pseudocapacitive behavior of the electrode due to the oxidation of the catalyst surface, caused by the current onset. Also because the potentials in Figures 4a and S9 were below the thermoneutral oxygen evolution potentials while a significant current was applied, it would be expected that charge is consumed by the oxidation of the surface.

The pseudocapacitive contributions were estimated for each current step in all measurements using the potential difference between the 1.1 V vs RHE standby steps and the maximum potential reached in each current step. The pseudocapacitance of the surface was calculated using the current between 1.0 and 1.2 V vs RHE (below thermodynamic OER potential) in the initial LSVs at 20 mV s^{-2} for each measurement. A more detailed description is available in the SI. From this, the relative pseudocapacitive contributions to the overall measured charge can be estimated, which are visible in Figure S10. The pseudocapacitive contribution to the total charge increased with the number of cycles since the pulse durations decreased due to the constant time of applied current. The contribution for the static protocol (600 s × 1) was <1%, which increased to approximately 63% for the 3 s × 200 protocol.

Based on these calculations, Figure 4c shows the dissolution values normalized to the OER charge obtained from correcting the total charge by the contribution from surface oxidation. After pseudocapacitive correction, a trend is visible where the dissolution per OER charge increases with more and shorter cycles except for the 3 s × 200 protocol. Even though this was where the most significant correction occurred since the OER contributed less than 50% to the total current.

A possible reason why the OER charge normalized dissolution still decreases for the 3/3 s protocol compared to 6/6 s is that the transient dissolution could be affected by the short duration of the current/potential steps. This includes the duration of the standby step, which might require more time at 1.1 V vs RHE to at least partially reverse the surface state to the initial composition so that a subsequent current step can oxidize it again and lead to transient dissolution, as visible in Figure 3b.

For the dynamic stress tests, the electrochemical degradation, measured as the change in activity at 1.60 V vs RHE, interestingly showed a negative correlation with the degradation measured by dissolution. The activity changes in Figure S8 additionally trend-wise correlated well with the inverse of Figure 4b, showing the highest gain in activity for the dynamic protocol with the highest normalized dissolution due to transient conditions and pseudocapacitive contributions. The redox cycling with LPLs of 1.1 V vs RHE had a rather activating effect on the catalyst film compared to the static stress tests for the presented material and dynamic protocols.

Measurement results from AMS must, as far as possible, be compared to results from MEA testing to assess the predictive value of the experiments for the application.[4,5] Alia et al. showed in their study, similar to this one, the impact of pulsing durations in an AST on electrochemical performance losses on single full cell level.[26] They found a continued increase of losses in electrochemical performance for increasing cycling frequencies. Different 525 h long ASTs using 60/60 s, 30/30 s, 15/15 s, and 5/5 s square wave potential steps in a potential range of 1.45−2 V were applied, using loadings of 0.1 mg_{Ir} cm^{-2} of iridium oxide (Alfa Aesar), the same OER electrocatalyst as in this study. It was further claimed that the performance loss from frequent cycling in MEA was likely due to catalyst layer thinning from iridium dissolution and weakening of the catalyst/ionomer/membrane interface.[26]

The increasing full-cell performance losses from Alia et al. for shorter pulse durations correlate positively with the increasing dissolution values normalized to the OER charge shown in Figure 4b. Especially for the pulse durations in the range of 6−10 s, the use of the corrected OER charge instead of the total charge for dissolution normalization significantly improved the agreement with full cell performance loss trends, increasing the predictive value of the method. Since performance losses on the full cell level are the results of the degradation of all the existing components and their interfaces, other pulsing-dependent degradation effects may have an impact as well. Overall, the presented results strongly suggest that the assumption of 100% Faraday efficiency toward OER is not generally valid for dynamic protocols and depends on the number of pulses and their duration, as shown in Figure S10. This should be considered in future studies when normalizing dissolution to charge or calculating S-numbers for dynamic protocols. Otherwise, dissolution increases due to transient dissolution can be concealed by the calculation method of performance metrics, as visible in Figure 4.

The findings in our study further suggest that results, where dissolution per charge from dynamic versus static stress tests is compared, may need to be reevaluated with consideration for the pseudocapacitive contributions, particularly when using pulses in the 3−10 s range.[27] The comparison of Figure 4b,c shows that otherwise the dynamic versus static stability could be significantly overestimated.

Additionally, the comparison of dissolution per total charge for similar dynamic protocols might be affected since not only short pulsing durations but also other parameters will likely be relevant for comparisons. A change toward higher UPLs or lower LPLs for instance would increase the ΔV between standby and OER steps, which is proportional to the estimated pseudocapacitive charge. Also since the relationship between

https://doi.org/10.1021/acscatal.5c01464
ACS Catal. 2025, 15, 10336−10346

potential and current is nonlinear for the electrochemical reaction, the relative charge consumed by surface oxidation (Pseudocapacitance) versus OER might change with different UPLs. Different loadings or surface areas might affect the pseudocapacitive contributions relative to the OER as well, particularly when comparing different materials.

Future research should further clarify the relevance of pseudocapacitive currents for different protocols when simultaneously varying measurement parameters as mentioned above. Additionally, the direct measurement of time-dependent oxygen evolution using dedicated mass spectrometry setups would enable a more precise calculation of the Faraday efficiency toward OER and the stability number for dynamic stress tests.[43,44] More effort needs to be dedicated to comparing the effects of parameter variations on component behavior on different system levels as well. This is central to understanding how performance trends in AMS relate to full-cell behavior and accelerate component development that translates to performance on full cell level. For this, intermediate setups like gas diffusion electrodes could play an important role in benchmarking e.g., more realistic catalyst layers in an environment with reduced complexity.[45,46]

4. CONCLUSIONS

In this study, we investigated catalyst dissolution to shorten the time needed for the stability screening for a commercial iridium oxide electrocatalyst for OER using an SFC-ICP-MS. An identical charge approach was used to assess the effect of reduced test durations on the dissolution. It was found that the total dissolution per charge for the used iridium oxide could be maintained after shortening the stability screening by a factor of 5 compared to a 600 s current pulse at 1 mA cm^{-2} as a benchmark. The time-resolved dissolution measurement however revealed that the constant dissolution per total charge was not due to a proportional increase of dissolution rates with OER current density. Rather, the initial dissolution per current was increased for 1 mA cm^{-2} compared to 5 mA cm^{-2}, which we attributed to higher relative contributions from transient dissolution at the lower current density. The approximation of steady state dissolution during the longer 600 s protocol at 1 mA cm^{-2} compensated for the higher initial dissolution per current, resulting in similar total values. Further shortening of the stress test duration while maintaining the applied charge however led to increases in dissolution and particle detachment from the tested catalyst layer.

Additionally, the dissolution from dynamic versus static stress tests was studied. This was done by fragmenting a single current hold into a larger number of shorter square wave pulses while maintaining the cumulative time of the applied current. It was observed that dynamic stress tests caused an increase in total dissolution per charge compared to the static benchmark in all cases due to transient dissolution. The correction of total charge by a pseudocapacitive contribution from surface oxidation revealed that the dissolution per OER increased for higher frequencies down to 6/6 s pulses. The corrected dissolution values further correlated positively with full cell performance losses in the literature for similar protocols, supporting the predictive value of the applied method for dynamic stability testing. The results demonstrate that a Faraday efficiency toward OER of 100% can not generally be assumed for dynamic protocols.

Our study highlights the need for further investigation of the dissolution and surface state of different materials. Particularly for short pulses, which can benefit the development of high-throughput methods and the understanding of degradation under dynamic conditions, further insights into the behavior of oxidic versus metallic and mixed metal(oxide) catalysts are needed. The presented methodology for dynamic stress testing shows promises for bridging the gap between the aqueous model systems and full cells for catalyst stability testing and can serve as guidance for further research on OER electrocatalyst benchmarking.

■ ASSOCIATED CONTENT

Supporting Information

The Supporting Information is available free of charge at https://pubs.acs.org/doi/10.1021/acscatal.5c01464.

Detailed description of experimental protocols, ICP-MS measurement data, and electrochemical data (PDF)

■ AUTHOR INFORMATION

Corresponding Authors

Philipp L. Darge − *Helmholtz-Institute Erlangen-Nürnberg for Renewable Energy (IET-2), Forschungszentrum Jülich, 91058 Erlangen, Germany; Department of Chemical and Biological Engineering, Friedrich-Alexander-Universität Erlangen-Nürnberg, 91058 Erlangen, Germany;* orcid.org/0000-0003-0933-8406; Email: p.darge@fz-juelich.de

Dominik Dworschak − *Helmholtz-Institute Erlangen-Nürnberg for Renewable Energy (IET-2), Forschungszentrum Jülich, 91058 Erlangen, Germany;* orcid.org/0000-0002-7585-767X; Email: d.dworschak@fz-juelich.de

Authors

Nico C. Röttcher − *Helmholtz-Institute Erlangen-Nürnberg for Renewable Energy (IET-2), Forschungszentrum Jülich, 91058 Erlangen, Germany; Department of Chemical and Biological Engineering, Friedrich-Alexander-Universität Erlangen-Nürnberg, 91058 Erlangen, Germany*

Matej Zlatar − *Helmholtz-Institute Erlangen-Nürnberg for Renewable Energy (IET-2), Forschungszentrum Jülich, 91058 Erlangen, Germany; Department of Chemical and Biological Engineering, Friedrich-Alexander-Universität Erlangen-Nürnberg, 91058 Erlangen, Germany;* orcid.org/0000-0003-1041-5149

Karl J. J. Mayrhofer − *Helmholtz-Institute Erlangen-Nürnberg for Renewable Energy (IET-2), Forschungszentrum Jülich, 91058 Erlangen, Germany; Department of Chemical and Biological Engineering, Friedrich-Alexander-Universität Erlangen-Nürnberg, 91058 Erlangen, Germany;* orcid.org/0000-0002-4248-0431

Serhiy Cherevko − *Helmholtz-Institute Erlangen-Nürnberg for Renewable Energy (IET-2), Forschungszentrum Jülich, 91058 Erlangen, Germany;* orcid.org/0000-0002-7188-4857

Complete contact information is available at: https://pubs.acs.org/10.1021/acscatal.5c01464

Author Contributions

P.L.D.: Conceptualization (lead), Methodology (lead), Validation (lead), Formal analysis (lead), Investigation (lead), Writing—Original Draft (lead), Writing—Review and Editing (lead), Visualization (lead). N.C.R.: Software—Automation of RDM and Data Curation via SQL for SFC-ICP-MS (lead),

https://doi.org/10.1021/acscatal.5c01464
ACS Catal. 2025, 15, 10336−10346

Writing—Review and Editing (supporting). M.Z.: Methodology—Design of experiments and electrochemical protocols for SFC-ICP-MS (supporting), Writing—Review and Editing (supporting). K.J.J.M.: Conceptualization (supporting), Resources (lead), Writing—Review and Editing (supporting), Supervision (supporting), Funding acquisition (lead). S.C.: Resources (supporting), Writing—Review and Editing (supporting), Supervision (supporting). D.D.: Conceptualization (supporting), Formal analysis (supporting), Writing—Review and Editing (supporting), Supervision (lead), Project administration (lead).

Notes

The authors declare no competing financial interest.

■ ACKNOWLEDGMENTS

P.L.D., N.C.R., and D.D. thank the German Ministry for Education and Research (BMBF) for financial support within the project HyThroughGen (03HY108A). P.L.D. particularly thanks Gun D. Akkoc for his contributions to the construction of the SFC testing station and RDM/software supervision in the group, Jonas Möller for the continuous work on the LabVIEW software for SFC control, and Christian Göllner for advice regarding and management of the ICP-MS. Further, P.L.D. thanks Lena Fiedler for ICP-MS management and help with Au foil preparation and Christopher Behling for sharing his experience on SFC development in the preparation of this work.

■ REFERENCES

(1) Pham, C. V.; Escalera-López, D.; Mayrhofer, K.; Cherevko, S.; Thiele, S. Essentials of High Performance Water Electrolyzers—From Catalyst Layer Materials to Electrode Engineering. *Adv. Energy Mater.* **2021**, *11* (44), No. 2101998.

(2) Kumar, S. S.; Himabindu, V. Hydrogen Production by PEM Water Electrolysis – A Review. *Mater. Sci. Energy Technol.* **2019**, *2* (3), 442–454.

(3) Hydrogen IRENA, 2024. https://www.irena.org/Energy-Transition/Technology/Hydrogen. (accessed December 17, 2024).

(4) Zlatar, M.; Escalera-López, D.; Rodríguez, M. G.; Hrbek, T.; Götz, C.; Mary Joy, R.; Savan, A.; Tran, H. P.; Nong, H. N.; Pobedinskas, P.; Briega-Martos, V.; Hutzler, A.; Böhm, T.; Haenen, K.; Ludwig, A.; Khalakhan, I.; Strasser, P.; Cherevko, S. Standardizing OER Electrocatalyst Benchmarking in Aqueous Electrolytes: Comprehensive Guidelines for Accelerated Stress Tests and Backing Electrodes. *ACS Catal.* **2023**, *13* (23), 15375–15392.

(5) Ehelebe, K.; Escalera-López, D.; Cherevko, S. Limitations of Aqueous Model Systems in the Stability Assessment of Electrocatalysts for Oxygen Reactions in Fuel Cell and Electrolyzers. *Curr. Opin. Electrochem.* **2021**, *29*, No. 100832.

(6) U.S. Department of Energy Technical Targets for Proton Exchange Membrane Electrolysis, 2024. https://www.energy.gov/eere/fuelcells/technical-targets-proton-exchange-membrane-electrolysis. (accessed April 05, 2024).

(7) Jenewein, K. J.; Thienhaus, S.; Kormányos, A.; Ludwig, A.; Cherevko, S. High-Throughput Exploration of Activity and Stability for Identifying Photoelectrochemical Water Splitting Materials. *Chem. Sci.* **2022**, *13* (46), 13774–13781.

(8) Jenewein, K. J.; Akkoc, G. D.; Kormányos, A.; Cherevko, S. Automated High-Throughput Activity and Stability Screening of Electrocatalysts. *Chem. Catal.* **2022**, *2* (10), 2778–2794.

(9) Jenewein, K. J.; Torresi, L.; Haghmoradi, N.; Kormányos, A.; Friederich, P.; Cherevko, S. Navigating the Unknown with AI: Multiobjective Bayesian Optimization of Non-Noble Acidic OER Catalysts. *J. Mater. Chem. A* **2024**, *12* (5), 3072–3083.

(10) Kormányos, A.; Jenewein, K. J.; Cherevko, S. High-Throughput Workflows in the Service of (Photo)Electrocatalysis Research. *Trends Chem.* **2022**, *4* (6), 475–478.

(11) Pham, C. V.; Bühler, M.; Knöppel, J.; Bierling, M.; Seeberger, D.; Escalera-López, D.; Mayrhofer, K. J. J.; Cherevko, S.; Thiele, S. IrO2 Coated TiO2 Core-Shell Microparticles Advance Performance of Low Loading Proton Exchange Membrane Water Electrolyzers. *Appl. Catal., B* **2020**, *269*, No. 118762.

(12) Alia, S. M.; Anderson, G. C. Iridium Oxygen Evolution Activity and Durability Baselines in Rotating Disk Electrode Half-Cells. *J. Electrochem. Soc.* **2019**, *166* (4), F282–F294.

(13) Geiger, S.; Kasian, O.; Mingers, A. M.; Nicley, S. S.; Haenen, K.; Mayrhofer, K. J. J.; Cherevko, S. Catalyst Stability Benchmarking for the Oxygen Evolution Reaction: The Importance of Backing Electrode Material and Dissolution in Accelerated Aging Studies. *ChemSusChem* **2017**, *10* (21), 4140–4143.

(14) Edgington, J.; Deberghes, A.; Seitz, L. C. Glassy Carbon Substrate Oxidation Effects on Electrode Stability for Oxygen Evolution Reaction Catalysis Stability Benchmarking. *ACS Appl. Energy Mater.* **2022**, *5* (10), 12206–12218.

(15) Bernt, M.; Hartig-Weiß, A.; Tovini, M. F.; El-Sayed, H. A.; Schramm, C.; Schröter, J.; Gebauer, C.; Gasteiger, H. A. Current Challenges in Catalyst Development for PEM Water Electrolyzers. *Chem. Ing. Tech.* **2020**, *92* (1–2), 31–39.

(16) Hartig-Weiss, A.; Tovini, M. F.; Gasteiger, H. A.; El-Sayed, H. A. OER Catalyst Durability Tests Using the Rotating Disk Electrode Technique: The Reason Why This Leads to Erroneous Conclusions. *ACS Appl. Energy Mater.* **2020**, *3* (11), 10323–10327.

(17) El-Sayed, H. A.; Weiß, A.; Olbrich, L. F.; Putro, G. P.; Gasteiger, H. A. OER Catalyst Stability Investigation Using RDE Technique: A Stability Measure or an Artifact? *J. Electrochem. Soc.* **2019**, *166* (8), F458–F464.

(18) Tang-Kong, R.; Chidsey, C. E. D.; McIntyre, P. C. Reversible Decay of Oxygen Evolution Activity of Iridium Catalysts. *J. Electrochem. Soc.* **2019**, *166* (14), No. H712.

(19) Tovini, M. F.; Hartig-Weiß, A.; Gasteiger, H. A.; El-Sayed, H. A. The Discrepancy in Oxygen Evolution Reaction Catalyst Lifetime Explained: RDE vs MEA - Dynamicity within the Catalyst Layer Matters. *J. Electrochem. Soc.* **2021**, *168* (1), No. 014512.

(20) Spöri, C.; Falling, L. J.; Kroschel, M.; Brand, C.; Bonakdarpour, A.; Kühl, S.; Berger, D.; Gliech, M.; Jones, T. E.; Wilkinson, D. P.; Strasser, P. Molecular Analysis of the Unusual Stability of an IrNbOx Catalyst for the Electrochemical Water Oxidation to Molecular Oxygen (OER). *ACS Appl. Mater. Interfaces* **2021**, *13* (3), 3748–3761.

(21) Cherevko, S.; Reier, T.; Zeradjanin, A. R.; Pawolek, Z.; Strasser, P.; Mayrhofer, K. J. J. Stability of Nanostructured Iridium Oxide Electrocatalysts during Oxygen Evolution Reaction in Acidic Environment. *Electrochem. Commun.* **2014**, *48*, 81–85.

(22) Cherevko, S.; Zeradjanin, A. R.; Topalov, A. A.; Kulyk, N.; Katsounaros, I.; Mayrhofer, K. J. J. Dissolution of Noble Metals during Oxygen Evolution in Acidic Media. *ChemCatChem.* **2014**, *6* (8), 2219–2223.

(23) Cherevko, S.; Geiger, S.; Kasian, O.; Mingers, A.; Mayrhofer, K. J. J. Oxygen Evolution Activity and Stability of Iridium in Acidic Media. Part 1.—Metallic Iridium. *J. Electroanal. Chem.* **2016**, *773*, 69–78.

(24) Alia, S. M.; Rasimick, B.; Ngo, C.; Neyerlin, K. C.; Kocha, S. S.; Pylypenko, S.; Xu, H.; Pivovar, B. S. Activity and Durability of Iridium Nanoparticles in the Oxygen Evolution Reaction. *J. Electrochem. Soc.* **2016**, *163* (11), No. F3105.

(25) Geiger, S.; Kasian, O.; Ledendecker, M.; Pizzutilo, E.; Mingers, A. M.; Fu, W. T.; Diaz-Morales, O.; Li, Z.; Oellers, T.; Fruchter, L.; Ludwig, A.; Mayrhofer, K. J. J.; Koper, M. T. M.; Cherevko, S. The Stability Number as a Metric for Electrocatalyst Stability Benchmarking. *Nat. Catal* **2018**, *1* (7), 508–515.

(26) Alia, S. M.; Stariha, S.; Borup, R. L. Electrolyzer Durability at Low Catalyst Loading and with Dynamic Operation. *J. Electrochem. Soc.* **2019**, *166* (15), No. F1164.

https://doi.org/10.1021/acscatal.5c01464
ACS Catal. 2025, 15, 10336–10346

(27) Spöri, C.; Brand, C.; Kroschel, M.; Strasser, P. Accelerated Degradation Protocols for Iridium-Based Oxygen Evolving Catalysts in Water Splitting Devices. *J. Electrochem. Soc.* **2021**, *168* (3), No. 034508.
(28) Knöppel, J.; Möckl, M.; Escalera-López, D.; Stojanovski, K.; Bierling, M.; Böhm, T.; Thiele, S.; Rzepka, M.; Cherevko, S. On the Limitations in Assessing Stability of Oxygen Evolution Catalysts Using Aqueous Model Electrochemical Cells. *Nat. Commun.* **2021**, *12* (1), No. 2231.
(29) Milosevic, M.; Böhm, T.; Körner, A.; Bierling, M.; Winkelmann, L.; Ehelebe, K.; Hutzler, A.; Suermann, M.; Thiele, S.; Cherevko, S. In Search of Lost Iridium: Quantification of Anode Catalyst Layer Dissolution in Proton Exchange Membrane Water Electrolyzers. *ACS Energy Lett.* **2023**, *8*, 2682−2688.
(30) Edgington, J.; Seitz, L. C. Advancing the Rigor and Reproducibility of Electrocatalyst Stability Benchmarking and Intrinsic Material Degradation Analysis for Water Oxidation. *ACS Catal.* **2023**, *13* (5), 3379−3394.
(31) Alia, S. M.; Reeves, K. S.; Cullen, D. A.; Yu, H.; Kropf, A. J.; Kariuki, N.; Park, J. H.; Myers, D. J. Simulated Start-Stop and the Impact of Catalyst Layer Redox on Degradation and Performance Loss in Low-Temperature Electrolysis. *J. Electrochem. Soc.* **2024**, *171* (4), No. 044503.
(32) Escalera-López, D.; Czioska, S.; Geppert, J.; Boubnov, A.; Röse, P.; Saraçi, E.; Krewer, U.; Grunwaldt, J.-D.; Cherevko, S. Phase- and Surface Composition-Dependent Electrochemical Stability of Ir-Ru Nanoparticles during Oxygen Evolution Reaction. *ACS Catal.* **2021**, *11* (15), 9300−9316.
(33) Alia, S. M.; Reeves, K. S.; Yu, H.; Park, J. H.; Kariuki, N. N.; Kropf, A. J.; Myers, D. J.; Cullen, D. A. Catalyst-Specific Accelerated Stress Tests in Proton Exchange Membrane Low-Temperature Electrolysis for Intermittent Operation. *J. Electrochem. Soc.* **2024**, *171* (2), No. 024505.
(34) Cherevko, S.; Geiger, S.; Kasian, O.; Mingers, A.; Mayrhofer, K. J. J. Oxygen Evolution Activity and Stability of Iridium in Acidic Media. Part 2.—Electrochemically Grown Hydrous Iridium Oxide. *J. Electroanal. Chem.* **2016**, *774*, 102−110.
(35) Spöri, C.; Kwan, J. T. H.; Bonakdarpour, A.; Wilkinson, D. P.; Strasser, P. The Stability Challenges of Oxygen Evolving Catalysts: Towards a Common Fundamental Understanding and Mitigation of Catalyst Degradation. *Angew. Chem., Int. Ed.* **2017**, *56* (22), 5994−6021.
(36) Kulyk, N.; Cherevko, S.; Auinger, M.; Laska, C.; Mayrhofer, K. J. J. Numerical Simulation of an Electrochemical Flow Cell with V-Shape Channel Geometry. *J. Electrochem. Soc.* **2015**, *162* (12), No. H860.
(37) Topalov, A. A.; Katsounaros, I.; Auinger, M.; Cherevko, S.; Meier, J. C.; Klemm, S. O.; Mayrhofer, K. J. J. Dissolution of Platinum: Limits for the Deployment of Electrochemical Energy Conversion? *Angew. Chem., Int. Ed.* **2012**, *51* (50), 12613−12615.
(38) Schuppert, A. K.; Topalov, A. A.; Katsounaros, I.; Klemm, S. O.; Mayrhofer, K. J. J. A Scanning Flow Cell System for Fully Automated Screening of Electrocatalyst Materials. *J. Electrochem. Soc.* **2012**, *159* (11), No. F670.
(39) Klemm, S. O.; Topalov, A. A.; Laska, C. A.; Mayrhofer, K. J. J. Coupling of a High Throughput Microelectrochemical Cell with Online Multielemental Trace Analysis by ICP-MS. *Electrochem. Commun.* **2011**, *13* (12), 1533−1535.
(40) Kovács, M. M.; Fritsch, B.; Lahn, L.; Bachmann, J.; Kasian, O.; Mayrhofer, K. J. J.; Hutzler, A.; Dworschak, D. Electrospun Iridium-Based Nanofiber Catalysts for Oxygen Evolution Reaction: Influence of Calcination on Activity−Stability Relation. *ACS Appl. Mater. Interfaces* **2024**, *16*, 52179−52190.
(41) Zeng, F.; Mebrahtu, C.; Liao, L.; Beine, A. K.; Palkovits, R. Stability and Deactivation of OER Electrocatalysts: A Review. *J. Energy Chem.* **2022**, *69*, 301−329.
(42) McCrory, C. C. L.; Jung, S.; Peters, J. C.; Jaramillo, T. F. Benchmarking Heterogeneous Electrocatalysts for the Oxygen Evolution Reaction. *J. Am. Chem. Soc.* **2013**, *135* (45), 16977−16987.
(43) Zheng, Y.-R.; Vernieres, J.; Wang, Z.; Zhang, K.; Hochfilzer, D.; Krempl, K.; Liao, T.-W.; Presel, F.; Altantzis, T.; Fatermans, J.; Scott, S. B.; Secher, N. M.; Moon, C.; Liu, P.; Bals, S.; Van Aert, S.; Cao, A.; Anand, M.; Nørskov, J. K.; Kibsgaard, J.; Chorkendorff, I. Monitoring Oxygen Production on Mass-Selected Iridium−Tantalum Oxide Electrocatalysts. *Nat. Energy* **2022**, *7* (1), 55−64.
(44) Kasian, O.; Grote, J.-P.; Geiger, S.; Cherevko, S.; Mayrhofer, K. J. J. The Common Intermediates of Oxygen Evolution and Dissolution Reactions during Water Electrolysis on Iridium. *Angew. Chem., Int. Ed.* **2018**, *57* (9), 2488−2491.
(45) Geuß, M.; Milosevic, M.; Bierling, M.; Löttert, L.; Abbas, D.; Escalera-López, D.; Lloret, V.; Ehelebe, K.; Mayrhofer, K. J. J.; Thiele, S.; Cherevko, S. Investigation of Iridium-Based OER Catalyst Layers in a GDE Half-Cell Setup: Opportunities and Challenges. *J. Electrochem. Soc.* **2023**, *170* (11), No. 114510.
(46) Geuß, M.; Löttert, L.; Böhm, T.; Hutzler, A.; Mayrhofer, K. J. J.; Thiele, S.; Cherevko, S. Quantification of Iridium Dissolution at Water Electrolysis Relevant Conditions Using a Gas Diffusion Electrode Half-Cell Setup. *ACS Catal.* **2024**, *14*, 11819−11831.

https://doi.org/10.1021/acscatal.5c01464
ACS Catal. 2025, 15, 10336−10346